æ

8. EVOLUTIONARY SCALING LAWS IN CELL BIOLOGY

1 September 2020

Cells vary widely in terms of shape, physiological properties, metabolic features, and internal architecture. Of particular importance is cell size, which influences a myriad of physical factors, ranging from nutrient uptake to internal transport, with variation among species likely driven by a variety of selective forces, including size-selective predators, buoyancy, resistance to flow dynamics, and osmotic pressure. Among the most well-studied unicellular species, cell volumes vary by approximately eleven orders of magnitude, 10^{-3} to 10^{8} μm^3, across the Tree of Life, with up to 10^{7}-fold differences within major phylogenetic groups (Figure 8.1). By comparison, the range in size between the smallest and largest mammals, a bumblebee bat vs. a blue whale, is just eight orders of magnitude. On average, prokaryotic cells are smaller than those of eukaryotic species, but some eukaryotes have cell volumes smaller than the average bacterium.

There are a few striking exceptions at the large end of the scale not shown in the figure. For example, the unicellular green alga *Acetabularia* is up to 10 cm in length and contains just a single nucleus, but has a complex architecture similar to that of a vascular plant. A multinucleate green alga *Caulerpa* produces complex holdfasts, stalks, and fronds up to meters in length, despite being unicellular. *Gromia sphaerica,* a testate amoeba that lives on marine sediments at depths of > 1 km, produces cells up to 4 cm in diameter. There are also giant bacteria. The marine-sediment bacterium *Thiomargarita* approaches 10^{9} μm^3 in size, and *Epulopiscium,* a gut symbiont associated with surgeonfish, has a volume well over 10^{6} μm^3.

Cell size is a major organizing factor in biology, with a wide array of cellular features scaling in predictable size-dependent manners across the Tree of Life. The scaling relationships aren't necessarily linear, but they often unfold in ways that transcend the boundaries between major phylogenetic groups, even between bacteria and eukaryotes. Such patterns are often called "laws of nature" or "rules of life," and if nothing else, they identify strict limits on what evolution has been able to achieve in the natural world. The question is why? Are absentee combinations of trait values a consequence of biophysical and/or biochemical constraints, or are certain combinations simply too disharmonious to be promoted by selection, or do both play a role?

The most notable of cell biology's scaling laws, the ways in which bioenergetic features relate to cell volume, constitute the primary subject matter of this chapter, although numerous relationships for other types of traits will be explored in subsequent chapters. The focus here is on the *evolutionary* scaling of traits with size across species. There are equally compelling questions regarding scaling rela-

tionships on nonevolutionary timescales (Marshall 2020), e.g., cellular responses to nutritional status, temperature, and other physical/chemical factors. Ultimately, we wish to know whether long-term evolutionary trajectories reflect within-species developmental responses to the environment. These issues will start to be addressed in the following chapter.

Before proceeding, a simple overview of the ways in which scaling laws are expressed and interpreted mathematically is in order. Using this framework, a number of general scaling relationships regarding energy acquisition and growth will then be summarized. This will be followed by an overview of the possible evolutionary mechanisms that have driven such patterns, and their implications for understanding the consequences of the prokaryote-eukaryote transition.

Describing Allometric Relationships

The description of a scaling relationship between two traits demands a statistical approach, as the twin goals are generally to quantify the average pattern and degree of noise in the response of one trait that corresponds to a change in the other. The relationship may be positive or negative, but provided a proportional change in one trait is associated with a constant proportional change in the other, a scaling relationship can be succinctly written in the form of a simple, two-parameter power function,

$$z = \alpha S^{\beta} + e, \tag{8.1a}$$

where in this case z is the measured phenotype of interest, S is a measure of organism size (usually mass or volume), α is a normalization constant (giving the expected value of z when $S = 1$), and β is the scaling coefficient. Equation 8.1a indicates that, on average, a two-fold change in S elicits a 2^{β}-fold change in z. The e term in Equation 8.1a is usually left out of such expressions (and will be from here on), as it is a random deviation between observed and predicted values with an average value of zero.

There is an elegant simplicity to power functions, as they exhibit linear form when z and S are jointly transformed logarithmically. On a log scale, Equation 8.1a becomes

$$\log(z) = \log(\alpha) + \beta \log(S), \tag{8.1b}$$

providing a simple basis for estimating the parameters α and β with linear-regression analysis. This linearity applies regardless of the logarithmic scale employed, e.g., to the base 10 as generally used here (denoted as log), or on the scale of natural logarithms (denoted as ln). First popularized by Thompson (1917) and Huxley (1932), power-function scalings in biology are generally referred to as allometric functions, with $\beta = 1$ denoting an isometric relationship. If β is positive but < 1, then z becomes proportionally smaller with increasing S, as $z/S = \alpha S^{\beta-1}$, with the exponent $\beta - 1$ being negative; this implies sublinear or hypometric scaling. In contrast, $\beta > 1$ implies supralinear or hypermetric scaling.

As will be seen below, cell biology is well-endowed with features that are reasonably described by Equation 8.1b as a first-order approximation. In principle, although rarely relied upon, more complex functions are possible. For example, β

could be a function of S. It should be noted, however, that the scales on which biological traits are measured are generally arbitrary, and even when a particular measure does not strictly adhere to the form of Equation 8.1a, a variety of mathematical transformations to a new scale can often lead to behavior consistent with the simplest power-law form (Lynch and Walsh 1998; Frank 2016).

Regressions of trait values on body (cell) mass with slopes approximating multiples of 1/3 raise the possibility of simple geometric explanations. For example, $\beta = 1$ suggests a mechanism directly proportional to the mass of cellular material, $\beta = 2/3$ suggests a mechanism related to surface area (because area is a function of the square and mass is a function of the cube of a length measurement), and $\beta = 1/3$ suggests a mechanism related to a linear dimension of the organism. As early investigators found numerous regression-coefficient *estimates* to be in the neighborhood of $x/3$ (where x is an integer value, usually 2 or 3), there was a tendency to assume they were exactly $x/3$ and then embark on generalized mechanistic explanations for the observed patterns. Even at an early stage in these kinds of studies, discomfort was expressed with the generality of various hypotheses (e.g., von Bertalanffy 1957), although the tradition of searching for general scaling relationships and explanations for them continues today, with a tendency to view significant deviations as annoying secondary effects. As will be discussed below, for example, much attention has been given to the idea that allometric coefficients are actually functions of $x/4$ rather than $x/3$. In light of the usual uncertainties in statistical analyses, however, it is often hard to justify one of these scalings versus the other. Is, for example, an estimated coefficient of $\beta = 0.29$ more consistent with $1/3 \simeq 0.33$ or $1/4 = 0.25$ scaling?

Scaling Laws in Cellular Bioenergetics

The vast majority of work on biological scaling relationships has been performed by ecologists striving to understand the basic energetic features of ecosystems, usually with a focus on their constituent multicellular taxa (e.g., Burger et al. 2019; Hatton et al. 2019). Our attention will be confined to the attributes of species that normally live as single cells. Nonetheless, as will be discussed in Chapter 25, there are intriguing extensions of the results covered here to multicellular lineages.

Comparative studies across the Tree of Life have identified numerous power-law scalings of biological features with cell size. Several such patterns were encountered in Chapter 7 – the slightly less than linear proportionality between cell dry weight and cell volume; the decline in the fractional contribution of DNA to total cellular biomass with increasing cell size; and the sublinear increase in the number of molecules per cell with cell size.

Strong correlational patterns imply strong constraints, and a key challenge for evolutionary cell biology is to determine their mechanistic basis. At least three nonmutually exclusive classes of explanations always merit consideration: 1) inevitable outcomes of biophysical / biochemical limitations; 2) consequences of evolutionary channeling towards particular combinations of trait values that maximize fitness; and/or 3) reflections of drift barriers beyond which the efficiency of selection is compromised (Chapter 4).

Metabolic rate. In any discussion of size scaling of biological traits, it is appropriate to start with metabolic-rate data, as no trait has been more widely measured phylogenetically. In a statement that quickly became canonized as "Kleiber's Law," Kleiber (1932, 1947) argued that the total metabolic rate of an organism (typically measured as the rate of oxygen consumption) scales as the 3/4 power of body mass. His original analyses were largely derived from observations on vertebrates, and considerable subsequent research has led to a substantially altered view.

Nonetheless, West et al. (1997, 1999, 2002) have promoted the idea that quarter power-law scalings constitute universal laws relevant to not just metabolic rate but to a wide array of additional organismal features across the entire Tree of Life. The novelty of their conclusions derives from the concept of fractal delivery systems (e.g., hierarchical branching networks of capillaries or leaf veins) for nutrients and respiratory gases, but the details of the underlying derivations will not be pursued here for several reasons. First, it is unclear how the features of a branching delivery network would apply to single cells. Second, a number of questionable mathematical assumptions underlying the fractal models have been highlighted (Dodds et al. 2001; Banavar et al. 2002; Kozłowski and Konarzewski 2004, 2005; Chaui-Berlinck 2006; Apol et al. 2008), which despite the originators' valiant efforts (Brown et al. 2005; Savage et al. 2007) have not been dissipated. Third, comparative data in protists yield a power-law relationship between cell surface area and volume with an exponent quite close to 3/4 (Fenchel 2014), contrary to the naive expectation of 2/3. Such behavior is a consequence of cell shapes shifting to flatter forms as species increase their average cell volumes. This means that, aside from the potential mathematical issues with the fractal-based model, the predicted scaling does not differ uniquely from that of a surface-area constraint model.

The most significant issue here is that for metabolic rates, one general power function does not apply across the Tree of Life. Not only is the allometric coefficient for metabolic rate often unequal to 3/4, but the regression appears to be nonlinear (Zeuthen 1953). With dry weight/cell being the measure of size, DeLong et al. (2010) found the allometric slope for metabolic rate for heterotrophic bacteria to be ~ 2.0 and for unicellular eukaryotes is ~ 1.1, with the same scaling found whether cells are active and well-nourished or inactive and starved. Using updated cell size measurements from Lynch et al. (2020), the allometric slopes for the two groups are more on the order of 1.3 and 1.0 (Figure 8.2), but the two estimates are not significantly different (Figure 8.2). Thus, although there is little overlap in cell sizes between the two groups, a hypothesis of complete continuity of scaling across both groups cannot be ruled out, and this leads to the prediction of an isometric relationship (with slope = 1.0). As these discrepancies with the 3/4 rule have been made repeatedly in other studies (Dodds et al. 2001; Kozłowski and Konarzewski 2005; Glazier 2015a,b), it is unclear why the universality of 3/4 power-law scaling continues to be promoted (West 2017).

Although metabolic rate is a classical physiological measurement, readily estimated as the rate of oxygen consumption or heat dissipation, its cell biological interpretation is generally far from clear. Total metabolic-rate measurements quantify the burning of carbon sources, but provide no information on the extent to which energy is converted to biomass production (growth and reproduction), the key targets of natural selection. Given the isometric relationship noted above, di-

viding cellular metabolic rate by cell mass implies that the rate of energy utilization per unit mass is essentially independent of size in unicellular species. Taken at face value, assuming that metabolic rate is somehow proportional to the rate of biomass production, this might suggest that cell-division rates would be nonresponsive to cell size. As discussed further below, this expectation is not fulfilled.

Lifetime energy requirements of a cell. Natural selection advances adaptations that enhance an organism's energetic capacity, either directly via growth and reproduction or indirectly via survivorship. However, adaptations themselves incur baseline construction and maintenance costs, and unless the benefits are sufficiently greater than the energetic costs, natural selection will be ineffective. To understand the capacity of natural selection to incorporate adaptive modifications, we require information on the net energetic costs and benefits relative to the total cellular energy budget (the summed costs of construction and maintenance per cell lifetime). This ratio provides a measure of the degree to which a cellular modification can be perceived by selection as opposed to being overwhelmed by the power of random genetic drift and accumulating by mutation pressure (Chapters 6 and 17). Thus, any evaluation of the relative cost of a genomic/cellular modification must start with a consideration of the total cellular energy requirements per cell cycle.

These total cellular requirements partition into components associated with: 1) baseline maintenance and survival; and 2) production of the essential parts of daughter cells (growth and reproduction). The numerous maintenance needs of a cell include energy invested in mRNA and protein production and processing, osmoregulation, intracellular transport, signal transduction, motility, and DNA repair. As the length of the cell cycle is prolonged, e.g., owing to resource limitation, the contribution of the maintenance requirement will grow approximately linearly with the time between cell divisions, whereas the contribution involving the construction of new parts (a roughly one-time investment) will remain approximately constant. As a consequence, the total lifetime energetic requirements of a cell (from birth to fission) will typically increase as growth conditions decline, eventually reaching the break point where resources are just sufficient for maintenance (with nothing left for allocation to reproduction).

A powerful approach that allows an empirical partitioning of maintenance and growth requirements of an organism relies on estimates of the consumption rate of an energy-limiting resource at different cell-division rates (Foundations 8.1). For cells that can be grown on a defined medium in a continuous-flow chemostat (Figure 8.3), the rate of resource consumption per cell can be estimated from the difference in resource concentration between the inflow and outflow, the known cell density (which reaches an equilibrium in the growth chamber), and the flow rate. Conversion of resource consumption to ATP yield (the universal energy currency of cells) requires knowledge of the metabolic pathways through which the substrate passes (Tempest and Neijssel 1984; Russell and Cook 1995).

The elegance of a continuous-flow culture is that an equilibrium cell-division rate is rapidly achieved, which is simply equal to the dilution rate of the chemostat. If the rate of resource consumption per cell is determined at several cell-division rates, a plot of the former vs. the latter is expected to yield a straight line, with the slope providing an estimate of the amount of resource consumed to produce a new cell,

and the intercept (denoting the point at which resource consumption is insufficient to support growth) providing a measure of baseline metabolic requirements (Figure 8.3). Pioneered by Bauchop and Elsden (1960), this regression approach is often called a Pirt (1982) plot.

The general procedure has been applied to enough organisms to reveal some broad generalizations (Figure 8.4). First, the basal metabolic rate (normalized to a constant temperature of 20°C for all species) scales almost linearly with cell volume across both bacteria and eukaryotes, with an allometric relationship of

$$C_M = 0.39V^{\,0.88}, \tag{8.2a}$$

where C_M is in units of 10^9 molecules of ATP/cell/hour, and cell volume V is in units of μm^3. Second, the scaling of the growth requirement per cell is even closer to linearity with respect to cell volume (i.e., with an exponent near 1.0),

$$C_G = 26.92V^{\,0.96}, \tag{8.2b}$$

where C_G is in units of 10^9 molecules of ATP/cell. If one further considers that a portion of eukaryotic cell volume is associated with vesicles and therefore relatively inert biologically, the regressions on active (or "effective") cell volumes might yield modified allometric scaling coefficients. Unfortunately, little information is available on the scaling of vacuolar volume with total cell size, although an analysis for photosynthetic cells suggests $\sim 89\%$ active volume for a 1-μm^3 cell, declining to $\sim 58\%$ in a 10^4-μm^3 cell (Okie 2013). This matter aside, Equations 8.2a,b still provide a highly useful quantitative statement on the cell-size dependence of maintenance and construction costs. Notably, both the maintenance and growth relationships scale in an apparently continuous fashion across bacteria and eukaryotes, despite the substantial difference in cell contents between the groups. On the one hand, eukaryotic cells contain internal lipid membranes, which are energetically expensive, but on the other hand, such cells are less densely packed with biomaterials (Chapter 7).

The total cost of building a cell is

$$C_T \simeq C_G + t_d C_M, \tag{8.2c}$$

where t_d is the cell-division time in hours. The relationships in Equations 8.2a,b then imply that provided $t_d < 67V^{0.1}$ hours (assuming 20°C), the contribution from cell growth dominates. The preceding relationships will prove useful in subsequent chapters as we attempt to determine the costs of various cellular features relative to a cell's entire energy budget.

The speed limit on cell-division rates. Natural selection is based on genotypic differences in rates of genome transmission on an absolute time scale. Thus, fitness ultimately depends not just on the rate of resource acquisition, but on the rate at which assimilated resources are transformed into new cells, as opposed to being burned in nonproductive activities. Thousands of studies have been performed on the growth rates of various species under a multitude of conditions, but given the diversity of approaches, the only fair comparison is to evaluate maximum known cell-division rates. Even then, the data must be normalized to a constant temperature

(as the latter influences all aspects of biology; Chapter 7), and there is no guarantee that studies on any particular species have indeed uncovered the optimal growth conditions.

With these caveats in mind, a broad survey of the literature suggests that the scaling of maximum cell-division rate and cell size (in units of dry weight per cell) is qualitatively different between heterotrophic bacteria and eukaryotes (Figure 8.5a). Here, the growth rate is measured as the maximum exponential rate of expansion $b_{\max} = \ln(2)/t_D$, where t_D is the population doubling time (in days). For bacteria, the scaling of this trait with cell size is positive with an allometric coefficient of 0.28 (SE = 0.07). Although there is considerable noise in the data, more than an order of magnitude range of variation in cell-division times for any specific cell size, this is in part due to sampling error. Moreover, even though the overall size range for which data are available is limited, the data certainly do not support the idea that large bacteria suffer from reduced rates of cell division, as might be expected if there was a surface area:volume constraint (below).

In contrast, unicellular eukaryotes exhibit weak, negative scaling of maximum growth rate with cell size. For amoeboid forms, ciliates, a broad group of heterotrophic flagellates, and dinoflagellates, the allometric scaling coefficients fall in the narrow range of -0.19 to -0.22. Despite this uniform size scaling over six orders of magnitude of cell size differences, the elevation of the power-law functions vary among groups, with ciliates having the highest growth rates and flagellates the lowest.

Unfortunately, there is very little overlap in the sizes of bacterial and eukaryotic cells in these analyses of heterotrophs, so it is unclear whether the observed shift in scaling behavior is a consequence of fundamental biological differences between groups or a reflection of a more general scaling relationship, with a global optimum size for cell-division rates being on the order of 10^{-6} μg. Although it may seem puzzling why all bacteria don't evolve to very large sizes and all unicellular eukaryotes to very small sizes, it should be remembered that total fitness is determined by the difference between birth and death rates, and that the optimum size for survivorship may differ greatly among environments.

One argument for a general shift in direction of scaling is that nonmodifiable components such as the plasma membrane occupy an increasingly large fraction of total cell volume as cells diminish to very small sizes, thereby restricting the amount of cytoplasm available for other scalable processes critical to cell growth. In a general review of marine phytoplankton, Raven (1986) argued that there is a general reversal in the scaling of cell-division times at a cell volume of ~ 30 μm^3, which equates to an approximate cell dry weight of 10^{-5} μg, close to the area of overlap in size of bacterial and eukaryotic heterotrophs in Figure 8.5a. Although a similar argument was made by Marañòn (2015; Marañòn et al. 2013), a broader comparative analysis does not support this sort of nonmonotonic scaling for phototrophs (Figure 8.5b). There is no relationship between $b_{\max}$ and cell size in cyanobacteria, and for the two phototrophs groups for which there are data on several dozens of species, green algae and diatoms, the allometric scaling coefficient is -0.09, which is about half that found for heterotrophs.

It bears emphasizing that the minimum cell-division times summarized in Figure 8.5, most of which are less than a day, are all derived from pure cultures grown under

optimized laboratory conditions. In nature, organisms may rarely if ever experience such conditions, commonly dividing at least one to two orders of magnitude more slowly than maximum rates. Indeed, many microbes inhabiting aquatic sediments are thought to have generation times on the order of several years, and in some cases even hundreds of years (Hoehler and Jørgensen 2013). In principle, such cells may often enter semi-dormant states with maintenance requirements lower than those implied in Figure 8.4, but little is known of this.

The preceding results permit three fairly general statements about the biology of cells. First, in both eukaryotes and bacteria, species with large cells tend to acquire biomass at higher *absolute* rates than do those with smaller cells. This follows from the fact that the energetic requirement for growth scales nearly linearly with cell volume (Figure 8.4), while cell-division rates scale much more weakly and even positively in the case of bacteria (Figure 8.5). For heterotrophic unicellular eukaryotes, the minimum cell-division time scales with cell volume with allometric coefficient 0.20. Thus, assuming that cell mass is nearly proportional to cell volume V (Chapter 7), the rate of incorporation of biomass scales as $\sim V^{0.96-0.20} = V^{0.76}$, whereas for bacteria, the rate of biomass accumulation scales more like $V^{0.96+0.28} \simeq V^{1.24}$. In both cases, the rate of production increases with cell size, but it does so supralinearly with size in bacteria but sublinearly in eukaryotic cells. It is this shift in scaling around a pivotal value of 1.0 that causes the shift in directionality of scaling of $b_{\max}$ between groups seen in Figure 8.5a, as $b_{\max}$ is a function of the absolute growth rate per unit biomass, i.e., the above scaling divided by V.

Second, returning to the results in the previous section, insight can be gained on the efficiency of conversion of assimilated energy into growth, C_G/C_T. To obtain, the lifetime cellular energy budget (C_T), we require an estimate of the cell-division time, t_d, as $C_T = C_G + t_d C_M$, where quantitative expressions are given for C_G (the cost of growth) and C_M (the cost of maintenance/day) as functions of cell volume (V) in Equations 8.2a,b. Defining t_d in units of days,

$$C_G/C_T \simeq \frac{1}{1 + 0.35 t_d V^{-0.08}}. \tag{8.3}$$

Here, the computations will be carried out just for bacteria, with only the final results being given for eukaryotic cells. Recalling from above that $t_d = \ln(2)/r_{\max}$, noting from the regression in Figure 8.5 that bacterial $r_{\max} \simeq 527 B^{0.28}$, where B is the dry weight per cell in μg, and using Equation 7.1 to express B in terms of V, leads to $t_d \simeq 0.055 V^{-0.26}$ (in units of days). Substitution of the latter expression into Equation 8.3 then leads to growth-efficiency estimates ranging from 0.92 to 0.99 for the range of bacterial cell volumes of 0.01 to 10 μm^3. Thus, for bacterial cells growing at maximum rates, the vast majority of assimilated energy is allocated to growth, increasingly so in cells of larger size. With poorer growth conditions (larger t_d), these efficiencies will necessarily decline. For example, with a tenfold increase in t_d, the corresponding efficiencies become 0.79 to 0.92, and with a 100-fold increase in t_d, they reduce to 0.10 to 0.54. Thus, a lower limit to bacterial cell size arguably results from the progressive increase in the fraction of energy intake that must be devoted to maintenance in the face of a relatively long cell-division time (Kempes et al. 2012).

Growth efficiencies are somewhat lower for eukaryotic cells. For heterotrophic eukaryotic flagellates, including dinoflagellates, growing at maximum rate, $t_d \simeq$

$0.18V^{0.17}$ days, and efficiencies decline from 0.93 to 0.83 for cell volumes of 10 to 10^6 μm^3. For amoeboid forms, the minimum cell-division time is $t_d \simeq 0.094V^{0.19}$ days, leading to a range for C_G/C_T of 0.95 to 0.84 for cell volumes of 100 to 10^8 μm^3. For ciliates, $t_d \simeq 0.036V^{0.20}$ days, and C_G/C_T ranges from 0.97 to 0.92 for cell volumes of 10^3 to 10^7 μm^3. Thus, when experiencing maximum growth capacity, most eukaryotic cells incorporate $> 90\%$ of assimilated energy into growth vs. maintenance, although the scaling of efficiency with cell volume is negative, in contrast to the situation in bacteria.

Third, the upper halves of the dashed ellipses in Figure 8.5a demarcate apparent absolute upper-bounds to cell-division rates (normalized to 20°C) that natural selection has been able to achieve. For heterotrophic eukaryotes at this temperature, no cell divides in < 1.7 hours, and no cell > 1 μg in dry weight divides in < 8 hours. No phototroph of any size, bacterial or eukaryotic, divides in < 4 hours at 20°C. On the other hand, at the same temperature, some large bacterial heterotrophs can divide in just 15 minutes.

The limits to natural selection imposed by the drift barrier. The classical dogma in physiological ecology is that scalings of bioenergetic features are unavoidable constraints of biochemistry and/or biophysics, as lucidly outlined by West (2017). Particularly common are arguments based on linear cell dimensions, which as noted above, lead to power-law behavior with exponents being multiples of 1/3 or 1/4, depending on whether the focus is on external surface area or internal delivery. However, although such hypotheses are based on what may appear to be reasonable arguments, the inferred supportive evidence derives from statistical analysis of patterns rather than on direct experimental evidence of mechanisms. A more fundamental problem is that neither one-third nor one-quarter power-law scalings provide general explanations for the scaling of bioenergetic traits in unicellular organisms.

With respect to bacterial growth rates, the data are noisy enough that the positive scaling is statistically consistent with an exponent of 1/5, 1/4, or 1/3. More striking are the opposite directions of scaling of maximum growth rate and efficiency with cell size in bacteria vs. eukaryotes. The scaling exponents for individual heterotrophic unicellular eukaryotic groups are mostly inconsistent with $-1/4$ power-law scaling, and all are below 0.25. Moreover, as will be discussed in Chapter 24, this pattern extends to multicellular animals. Thus, the overall pattern for heterotrophic eukaryotes is much more compatible with $-1/5$ than either $-1/4$ or $-1/3$ power-law scaling. For phototrophs, the scaling exponent is much weaker than $-1/5$, being closer to $-1/10$. The key point is that these patterns are incompatible with purely biophysical explanations, at least to the degree that they have been formulated to this point.

All of this suggests a need to evaluate the problem from an entirely different perspective. Shifting the view from biophysical constraints to limits on the evolutionary process, one possibility is that with increasing cell size, the efficiency of natural selection declines, owing to the associated reduction in effective population size (Chapter 4) and the likely reduction in the fitness effects of certain kinds of mutations (Chapter 17). If this hypothesis is correct, arguments that attempt to explain scaling patterns across the Tree of Life purely on the basis of physiological

and cell-geometric arguments will be incomplete, if not entirely misplaced. If, on the other hand, it could be shown that the population-genetic environment has no influence on scaling relationships, this would imply that the structure of cell biology is such that there is always a supply of mutations with sufficiently small and variable effects to universally bring things to their biophysical limits.

The intention here is not to promote the idea of precise 1/5 (or 1/10) power-law scaling relationships. Further empirical study of the distribution of mutations with small effects in various phylogenetic lineages will be necessary for that level of resolution. The main point is that an assumption of the unbridled power of natural selection is particularly questionable for traits related to growth rate and other bioenergetic features.

Recall from Chapter 4 that the key determinant of whether natural selection can eradicate a deleterious mutation with effect s is whether the ratio of the power of selection to the power of drift $s/(1/N_e) = N_e s$ exceeds 1.0, where N_e denotes the effective population size. There, it was further shown that N_e of a species scales with the -0.20 power of the size at maturity (Figure 4.3). This implies that species with larger cell sizes have reduced capacities to promote growth-rate promoting mutations and to eradicate growth-rate reducing mutations of small effects. As noted in Chapter 5 and further elaborated on in Chapter 17, the evidence is compelling that a large fraction of mutations have fitness effects (s) far below $|s| = 10^{-5}$, extending down to 10^{-10}, with the lower bound likely being lower in species with larger cell sizes. Because N_e in unicellular species is typically in the range of 10^6 to 10^9 individuals, this means that a substantial number of mutations with individually very mildly deleterious (i.e., growth-reducing) effects are free to accumulate in the genomes of species with relatively small N_e while still being subject to efficient purging in large-N_e species.

As discussed in Chapter 5, several genetic features determine how the efficiency of selection against mildly deleterious mutations scales with the demographic features of a population. Evaluation of these in a stepwise fashion shows how the progressive incorporation of natural genomic features can lead to the kinds of scaling outlined in Figures 8.5a,b. The simplest starting point assumes that selection operates on individual genetic loci independently of events occurring at other genomic locations. This requires either very high recombination rates or such small population sizes that cosegregating variants are never simultaneously present at multiple loci. Consider the situation in which each locus harbors two possible alleles, + and −, with the mutation rates from + to −, and vice versa, being u_{10} and u_{01}, and the + allele having advantage s. At small enough population sizes that $N_e s \ll 1$, the long-term average frequency of the favorable + allele is simply a function of the ratio of mutation rates, $u_{01}/(u_{01} + u_{10})$, but with increasing N_e, the increased efficiency of selection drives the mean frequency to 1.0 once $N_e s \gg 1$ (Figure 8.6a). Under this model, the transition between these two extremes occurs in a narrow (order of magnitude) range of N_e, with the neutral expectation holding for $N_e s \ll 0.05$ and an equilibrium frequency of the + allele near 1.0 being closely approximated when $N_e s \gg 5$. Thus, this simple model is inadequate to explain a consistent scaling of mean performance across several orders of magnitude of N_e.

Suppose, however, that there are multiple, completely linked loci with the same mutational and selection properties, with a haplotype's growth rate being deter-

mined in an additive fashion (proportional to the fraction of loci occupied by + alleles), and fitness being defined by a multiplicative (independent effects) fitness model, $(1-s)^{n_0} \simeq e^{-sn_0}$, where n_0 is the number of − alleles. In this case, it can take as many as five orders of magnitude of N_e to span the full range of equilibrium mean growth rate (Figure 8.6b). This shift in behavior is a consequence of selective interference among simultaneously segregating mutations – for populations of moderate size, there will be genetic variation among individuals in terms of the total number of + alleles harbored across loci, the result being that many new beneficial mutations will arise on suboptimal genetic backgrounds destined to eventual loss. At the largest population sizes, however, selection still keeps − alleles at very low frequencies at all genomic sites, reducing the effects of background interference.

Generally, it can be expected that fitness effects will vary among genomic sites, with sites with large effects being much rarer than sites with small effects (Chapter 5). In this case, with free recombination, the equilibrium mean performance (relative to the maximum possible) will be a mixture of the responses found for mutations with fixed effects. Three possibilities involving the four classes of mutations in Figure 8.6a are shown in Figure 8.6c: equal frequencies of all classes; and frequencies increasing with decreasing effects by factors of 10 and 100. Again, it can be seen that the full range of mean performance can scale out over the full range of N_e depending on the skew of the mixture distribution. Such behavior is a simple consequence of the sites with progressively smaller effects requiring increasingly high N_e for selection to promote their favorable alleles. This can be observed as the stepwise increment in mean performance in Figure 8.6c; a smoother transition would arise with a continuous distribution of site effects.

Finally, Figure 8.6d considers the situation in which different types of sites are completely linked. In this case, as a site with major effects becomes surrounded by increasing numbers of minor-effect sites, there is again a progressive decline in the rate of scaling of mean performance with N_e. Increasing numbers of minor-effect loci cause increased background interference for selection operating on the major-effect site, while also contributing more to the total maximum performance of the trait (diluting the overall influence of the major-effect site).

Without a detailed understanding of the fine-scaled distribution of genomic sites with different magnitudes of mutational effects, an explicit statement cannot be made on the exact form of scaling of mean performance with respect to N_e. However, for a trait like growth rate, it can be expected that essentially every nucleotide site influences performance in at least a small small way, and that there will be considerable variation among sites in terms of average effects and recombination rates. Because the plotted results encompass a wide range of plausible genetic properties, these analyses at least make clear that there is little justification for ignoring the possibility that the variation in the population-genetic environment (in this case the reduction in N_e associated with increased organism size) plays a significant role in defining relationships between maximum performance and organism size. For this not to be the case, mutations at all sites would have to have selection coefficients in excess of the largest $1/N_e$ (on the order of 10^{-4}), which is highly implausible.

Note that both N_e and the maximum growth rate in eukaryotes scale with the approximately -0.2 power of cell size. There are statistical uncertainties with both measures, and it is not the intention here to claim that both scalings have identical

parametric values. However, for explanatory purposes, it is convenient to consider what this would mean if true. Given the critical benchmark for effective selection of $N_e s = 1$, parallel scaling would require that a proportional increase in cell volume be accompanied by the same proportional increase in the load from effectively neutral (but mildly deleterious) growth-reducing mutations. In principle, this could occur if the fitness effects of mutations followed an approximately exponential distribution, which as discussed in Chapters 5 and 17 is plausibly supported by the existing data. For phototrophs (with -0.10 growth-rate scaling), however, for every x-fold increase in cell size, there would have to be a $x/2$-fold increase in the load of small-effect mutations. This, in turn, implies a less steep distribution of fitness effects of mutations in phototrophs, but it remains unclear why the scaling should be different among these two major groups.

Membrane Bioenergetics and the Prokaryote-Eukaryote Transition

As noted in Chapter 2, a peculiar historical feature of cell biology is the localization of the key machinery associated with energy production to lipid bilayers. The series of complexes known as the electron transport chain (ETC) couple the extraction of electrons from the oxidation of organic compounds with the export of hydrogen ions, creating a concentration gradient of the latter across the membrane. The biochemical details of this process are covered in all biochemistry texts, and will not be elaborated upon here. The salient issue is that the cross-membrane gradient in hydrogen-ion concentration driven by the ETC causes chemiosmotic pressure for the return movement of hydrogen ions through membrane-embedded ATP synthase complexes, which couple this mechanical energy to the production of ATP. One of the central differences between prokaryotes and eukaryotes is that in the former all of these events take place on the inner cell membrane, whereas in eukaryotes membrane bioenergetics has been relocated/restricted to the inner membranes of mitochondria (where they would have been present from the outset in the primordial mitochondrion; Chapter 23).

Under the assumption that energy production is limited by the number of ATP synthase complexes, which in turn is assumed to be limited by the availability of membrane-surface area in bacteria, Lane (2002, 2015, 2020; Lane and Martin 2010) argues that the endosymbiotic establishment of mitochondria freed eukaryotes of this constraint by providing effectively unlimited inner mitochondrial membranes. This assertion led to the further claim that the energetic boost made possible by mitochondria constituted a watershed moment in evolution by generating excess power essential to all things associated with eukaryogenesis. Under this view, the mitochondrion is not simply one of the many unique features of eukaryotes. Rather, it is the key feature that enabled the evolution of internal cell structure, large cell size, expanded genomes, multicellularity, sex, behavior, etc.

Before evaluating the likelihood of this scenario, a brief consideration of the surface-area problem is in order. The general formulae for several common cell shapes are provided in Table 8.1, where it can be seen that regardless of the shape, volume always increases with the cube of a linear dimension, whereas the surface area increases with the square of the linear measure. The surface-area to volume

ratio depends on shape, but it is always inversely related to a linear dimension of the cell.

Because the production of ATP in prokaryotes is highly dependent on complexes embedded in the plasma membrane, the geometric-constraint argument implies that if the cell surface is a limiting resource, there should be a reduction in energy production per unit volume with increasing cell size. However, the analyses in the previous section already shed doubt on this assertion, showing that increased cell size in bacterial species is associated with higher, not lower, maximum rates of growth. In contrast, mitochondria-bearing eukaryotes have lower energetic capacities than prokaryotes on a volumetric basis, and growth rates decline with with increasing cell size. This matters from an evolutionary perspective because it is the growth rate per unit volume, often called the specific growth rate, that determines the rate of gene flow into the next generation. Thus, observations on the growth-rate potential across the Tree of Life are contrary to the basic premise underlying the Lane hypothesis.

Table 8.1. Geometric features for cells of common shapes. Abbreviations: $r < \ell$, radii or half-widths for spheroids; h, full length of a cylinder or rod; $\alpha = h/r$ or ℓ/r. Note that for a rod, h is the length from one rounded tip to the other. The formula for the surface area of a spheroid is known as Knud Thomsen's approximation.

Shape	Surface Area (S)	Volume (V)	S/V
Sphere	$4\pi r^2$	$(4/3)\pi r^3$	$3/r$
Cylinder	$2\pi r(r+h)$	$\pi r^2 h$	$2(1+\alpha)/h$
Rod	$2\pi rh$	$\pi r^2[h-(2r/3)]$	$(2\alpha/r)/[\alpha-(2/3)]$
Prolate spheroid	$2.02\,\pi r^2(1+2\alpha^{1.61})^{0.63}$	$(4/3)\pi r^2\ell$	$(1.5/\ell)(1+2\alpha^{1.61})^{0.63}$

Energy production and the mitochondrion. A consideration of eukaryotic cell anatomy provides a more mechanistic view of why the total membrane energetic capacity of eukaryotic cells is nothing out of the ordinary. A key question is whether mitochondria do indeed endow eukaryotic cells with enhanced membrane surface area for the occupancy of ATP synthase. Although the situation at the time of first colonization of the mitochondrion is unknown, the iconic view of mitochondria being tiny, bean-shaped cellular inclusions is not generalizable. For example, many unicellular eukaryotes harbor just a single mitochondrion or one that developmentally moves among alternative reticulate states (e.g., Burton and Moore 1974; Rosen et al. 1974; Osafune et al. 1975; Biswas et al. 2003; Yamaguchi et al. 2011; Uwizeye et al. 2020). Such geometries necessarily have lower total surface areas than a collection of spheroids with similar total volumes. For the range of species that have been examined, many of which do have small individualized mitochondria, the total outer surface area of mitochondria per cell is generally on the order of the total area of the plasma membrane, with no observed ratio exceeding 5:1, and those for the smallest species being less than 1:5 (Figure 8.7a). Given the likely archaeal nature of the cell that hosted the primordial mitochondrion (Chapter 23), it is likely that

the starting condition resembled the situation in the smallest eukaryotes unless the host cell was extraordinarily large or the primordial mitochondria were unusually tiny.

Although the outer surface area of the mitochondrion has been the most common source of measurements, it is of less relevance than that of the inner membrane, where the ATP synthase complex sits. However, for the few species that have been investigated, the ratios of inner to outer membrane areas for mitochondria are modest – ∼5.0, 2.4, 2.5, and 5.2, respectively, in mammals, the green alga *Ochromonas,* the plant *Rhus toxicodendron,* and the ciliate *Tetrahymena* (summarized in Lynch and Marinov 2017). Moreover, the total surface areas of mitochondria substantially overestimate the real estate allocated to ATP synthase complexes, which are actually restricted to two rows on the narrow edges of the inner invaginations (called cristae), comprising $\ll 10\%$ of the total internal membrane area (Kühlbrandt 2015).

Three additional observations raise further questions as to whether membrane surface area is a limiting factor in ATP synthesis. First, multiple observations on the developmental responses of organelles to cell growth indicate that the total mitochondrial volume remains proportional to cell volume (Atkinson et al. 1974; Grimes et al. 1974; Posakony et al. 1977; Pelligrini 1980; Rafelski et al. 2012), and the same has been observed in the comparative analysis of protist species (Fenchel 2014). From the arguments in the preceding section, this implies that the surface area of mitochondria scales with the 2/3rds power of cell volume, and hence that mitochondrially generated power per cell volume declines as $V^{-1/3}$. Thus, if mitochondrial surface area limits cellular energy production, to maintain mitochondrial generating power capacity, the concentration of mitochondria would need to scale as $V^{1/3}$ rather than being volume independent. Second, only a fraction of bacterial membranes appears to be allocated to bioenergetic functions (Magalon et al. 2015), again shedding doubt on whether membrane area is a limiting factor for prokaryotic energy production. Third, as will be discussed more fully in Chapter 9, in every bacterial species for which data are available, growth in cell volume is exponential or close to it. This means that growth rates of individual bacterial cells increase with cell volume despite the reduction in the surface area:volume ratio.

Still further insight into this issue derives from the average packing density of ATP synthase for the few species with sufficient proteomic data (Lynch and Marinov 2017). For example, the estimated number of complexes in *E. coli* is ~ 3000, and the surface area of the cell is $\sim 16\ \mu\text{m}^2$. Based on the diameter of the molecule, a single ATP synthase in this species occupies $\sim 64\ \text{nm}^2$ (Lücken et al. 1990) of surface area, so the total set of complexes occupies $\sim 2\%$ of the cell membrane. Drawing from additional observations on four other diverse bacterial species, the overall average membrane occupancy of ATP synthase is just 1% in bacteria (Lynch and Marinov 2017).

This kind of analysis can be extended to the few eukaryotes for which data are available, noting that eukaryotic ATP synthases are slightly larger, with maximum surface area of $\sim 110\ \text{nm}^2$ (Abrahams et al. 1994; Stock et al. 1999). Although ATP synthase resides in mitochondria in eukaryotes, it is relevant to evaluate the fractional area that would be occupied were they to be located in the cell membrane. Such hypothetical packing densities are 5 to 7% for yeast and mammalian cells (Lynch and Marinov 2017). These observations suggest a $\sim$ 5-fold increase in

ATP synthase abundance with cell surface area in eukaryotes, but the data conform to a continuous allometric function with no dichotomous break between bacteria and eukaryotes (Figure 8.7b). Thus, this multifaceted set of observations is consistently contrary to the idea that the relocation of membrane bioenergetics endowed eukaryotes with enhanced growth efficiency beyond what would be expected of bacterial cells of similar size. Indeed, if there are any effects at all, they appear to be negative.

Cellular investment in ribosomes. The ribosome content of a cell provides a strong indicator of its bioenergetic capacity. Owing to the large number of proteins required to build the complex, ribosomes are energetically costly, and the number per cell within a species appears to be universally correlated with cellular growth rate, with low nutritional states being accompanied by reduced investments in ribosomes relative to components of the cell involved in nutrient uptake (Chapter 9). One might then expect variation in the translational capacity of cells of different species to reflect their intrinsic bioenergetic potential.

It was noted in Chapter 7 that the genome-wide total and mean number of transcripts per gene scale with cell volume as $V^{0.36}$ and $V^{0.28}$ respectively, and that the analogous scalings are $V^{0.93}$ and $V^{0.66}$ for proteins, with no dichotomous break between prokaryotes and eukaryotes (Lynch and Marinov 2015). As with the transcripts they process and the proteins they produce, the numbers of ribosomes per cell also appear to scale sublinearly with cell volume, in a continuous fashion across bacteria and unicellular eukaryotes, including cultured cells from multicellular species. In this case, the scaling is proportional to $V^{0.79}$ (Figure 8.8). Note that under the assumption that ribosomes produce proteins at approximately constant rates in different organisms, the scaling of protein production per volume would be $V^{0.79}/V = V^{-0.21}$. Thus, the cellular concentration of ribosomes matches the scaling of maximum growth rates with eukaryotic cell size outlined in Figure 8.5, reinforcing the idea of a negative scaling of biomass production rates with cell volume.

The mitochondrion as a driver of eukaryotic evolution. Lane (2015) and Lane and Martin (2010) have proposed a scenario for how the mitochondrion became established by a series of adaptive steps, arguing that the eukaryotic leap to increased gene number and cellular complexity, and a subsequent adaptive cascade of morphological diversification, "was strictly dependent on mitochondrial power." A similar argument was made by DeLong et al. (2010), and many others have repeated the narrative that eukaryogenesis and all of the associated downstream effects would be impossible without mitochondria.

However, as should now be clear, there is no evidence in support of this hypothesis, with diverse sets of comparative observations all leading to the opposite conclusion. Large bacterial cells do not suffer from reduced rates of biomass production, but eukaryotic cells do. There is not a quantum leap in the surface area of bioenergetic membranes in eukaryotes, nor is the idea that ATP synthesis is limited by total membrane surface area supported. Moreover, the numbers of ribosomes and ATP synthase complexes per cell, joint indicators of a cell's capacity to convert energy into biomass, scale with cell size in a continuous fashion both within and be-

tween bacterial and eukaryotic groups. In addition, as will be noted in subsequent chapters, the absolute costs of producing not only ribosomes but the remaining proteins in cells are substantially higher in eukaryotes than in bacteria, owing to the substantial increase in ribosome size, gene lengths, investment in nucleosomes, etc. Finally, there is the additional matter of the expense of building mitochondria, associated with the high biosynthetic costs of lipid bilayers (Chapter 15).

More will be discussed with respect to the origin of the mitochondrion in Chapter 23, but the idea that the mitochondrion engendered a bioenergetics revolution can be put to rest for now. The relocation of membrane bioenergetics to inner mitochondrial membranes may have endowed eukaryotes with novel possibilities for further remodeling of cellular features. But an enhanced capacity for transforming energy into biomass was not one of them.

Summary

- Cell volumes vary by approximately eleven orders of magnitude across the Tree of Life, with most being in the range 10^{-3} to 10^{8} μm^3 in volume. Although most prokaryotic cells are < 10 μm^3 in size, a few giants exceed 10^{9} μm^3, and a few unicellular eukaryotes with complex morphology are orders of magnitude larger.

- Species-specific mean phenotypes for various traits often scale in a continuous manner with cell size, suggesting substantial constraints on evolutionary diversification. A central goal of evolutionary cell biology is to determine the degree to which such patterns are simple consequences of biophysical constraints, selective disadvantages of discordant combinations, or outcomes of a drift barrier that increases with cell size.

- One of the most studied physiological traits is metabolic rate, which scales positively with cell volume, but does so in a nearly isometric fashion in unicellular species. Such behavior is inconsistent with the 2/3 or 3/4 power-law scaling often invoked in the literature. Despite their ease of acquisition, metabolic-rate measures provide little insight into the basic currency of natural selection, as they provide no information on the rate at which energy is converted into growth and reproduction.

- The energetic costs of both constructing and maintaining cells scale nearly isometrically with cell volume across the Tree of Life, despite the significant differences in cellular architectures between prokaryotes and eukaryotes. The biophysical/evolutionary determinants of the total costs remain to be determined.

- Maximum cell-division rates scale positively with cell size among heterotrophic bacterial species, but negatively among eukaryotic heterotrophs. Similarly, there is a directional shift in the efficiency of conversion of energy to growth in het-

erotrophic bacteria vs. unicellular eukaryotes, with growth efficiency being lowest in large eukaryotic cells, and highest in large prokaryotic cells.

- The precise mechanisms that define the upper limits to growth rate remain unresolved, but the case can be made that the negative scaling with cell size in eukaryotes is at least in part a consequence of the reduced efficiency of natural selection operating on growth-rate related mutations in organisms with progressively larger cell size. As cell size increases, and the effective population size decreases, a larger number of mild growth-rate reducing mutations are free to drift to fixation.

- It is commonly asserted that the establishment of the mitochondrion released the host eukaryotic cell from a surface area:volume constraint, eliciting a bioenergetic revolution. However, a diversity of observations, ranging from the scaling of energetic traits with cell size to the anatomy of mitochondria, are inconsistent with this hypothesis.

Foundations 8.1. The cost of building a cell. Cell-division rates are ultimately determined by the rate of acquisition of energy necessary to build a new cell. Arguably, the best currency to use in such analyses is units of ATP, as it is the hydrolysis of phosphate bonds in the conversion of ATP to ADP (and in some cases, ADP to AMP, or GTP to GDP) that delivers the vast majority of energy for cellular functions. In principle, with a solid enough understanding of biosynthetic pathways and the various inputs of cellular resources, one could calculate the total energy required to build a cell by summing over the demands for the replacement of proteins, nucleic acids, lipids, etc. However, energy transformation is not 100% efficient, cellular components turnover on time scales less than the life of a cell, and energy must be invested into additional maintenance functions. Thus, the total energy utilized by a cell before giving rise to two daughters must exceed the cost of producing the standing levels of cellular components. This total level of investment (maintenance plus construction) represents the net cost of building a cell.

Determining the quantity of interest here is generally difficult for cells growing in natural environments, as most heterotrophic organisms consume a variety of resources varying in energy content. Thus, most knowledge in this area is derived from the growth of organisms (virtually always microorganisms) in a defined medium with a single limiting carbon/energy source that enters a metabolic pathway with well-understood ATP-generating properties. If the organism can be grown in a chemostat (Figure 8.3a), it is straight-forward to calculate both the rate of cell division and the rate of substrate consumption, and therefore to obtain the ratio, i.e., the yield of cells per unit consumption.

Data derived from such analyses were the source of the information presented in the preceding chapter on yields of biomass per unit carbon consumption (Figure 7.8). However, as previously noted, the level of yield can depend on the nature of the carbon source, so a more meaningful measure focuses on a secondary calculation involving conversion to the yield per unit ATP hydrolysis. Such a measure is more generalizable, as it accounts for differences in energetic contents among alternative carbon sources.

A chemostat (Figure 8.3a) consists of a closed environment in which a sterilized resource-bearing medium is pumped in at a defined rate, with resource-depleted effluent (including the cells suspended within it) being eliminated at the same rate. If such a system is seeded with a pure population of a microbe, after several rounds of cell division, the population size will reach a steady state defined by the flow rate and the nutrient concentration. At this point, the population will have grown to a density at which the cell-division rate r equals the dilution rate d (i.e., the flow rate divided by the culture volume). The rate of resource consumption per cell is equal to the rate of loss of substrate (the flow rate times the concentration difference between the inflow and outflow) divided by the number of cells in the steady-state culture.

Joint insight into the maintenance and growth requirements of cells is acquired by culturing cells under different flow rates, which imposes different nutritional states as low and high dilution rates lead to high and low population densities (and hence low and high nutrient availabilities per cell). Assuming a constant rate of resource consumption per cell necessary for maintenance (C_M), the consumption rate (per unit time) at cell-division rate r (equivalent to the dilution rate d) can be written as

$$C = C_M + (r \cdot C_G) \tag{8.1.1}$$

where C_G measures the total growth-related consumption per cell division (Tempest and Neijssel 1984; Russell and Cook 1995). From a fitted least-squares regression of observed consumption rates C against growth rates r, the intercept and slope respectively estimate the cellular requirements for maintenance per unit time and growth per cell division, C_M and C_G (Figure 8.3b).

The total cost of producing a cell at any growth rate r can be obtained by multiplying the consumption rate C by the mean cell-division time, which is equivalent to the reciprocal of the cell division rate, $1/r$,

$$C_T = (C_M/r) + C_G, \tag{8.1.2}$$

Provided the assumption of a constant rate of basal metabolism independent of the growth rate is correct, this means that lifetime resource requirements are higher in slower-growing cells owing to the increased cumulative maintenance requirements under a longer lifespan.

In the preceding formula, the units associated with C_T and C_G are of the form (amount of resources consumed)/cell. Here, however, we are interested in defining C_T to be the number of ATP hydrolyses required to yield a new cell, so appropriate conversions need to be made. C_G is then defined as the total number of ATP hydrolyses consumed in the production of building blocks leading to an offspring cell (independent of time), and C_M as the number of ATPs utilized per cell per unit time for maintenance. The quantity $1/C_G$ is often denoted as $Y_{\max}$, as it represents the yield of cells per unit resource consumption that would occur in the absence of basal cellular requirements.

Although the general approach just taken assumes that metabolic requirements are constant, independent of the rate of growth, alternative formulations have been developed for the situation in which there is an additional metabolic cost to growth (Tempest and Neijssel 1984; Wieser 1994; Russell and Cook 1995). Note, however, that if maintenance costs are linearly related to the growth rate, this additional contribution is simply contained within the term C_G in Equation 8.1.1, but in principle, a term that is a nonlinear function (e.g., a quadratic) of r can be included. Although such alternative expressions can yield somewhat different interpretations on how energy is partitioned as a function of the growth environment, the total energy requirement observed at any particular growth rate remains unambiguous.

Literature Cited

Abrahams, J. P., A. G. Leslie, R. Lutter, and J. E. Walker. 1994. Structure at 2.8 A resolution of F1-ATPase from bovine heart mitochondria. Nature 370: 621-628.

Apol, M. E. F., R. S. Etienne, and H. Olff. 2008. Revisiting the evolutionary origin of allometric metabolic scaling in biology. Func. Ecol. 22: 1070-1080.

Atkinson, A. W. Jr., P. C. John, and B. E. Gunning. 1974. The growth and division of the single mitochondrion and other organelles during the cell cycle of *Chlorella,* studied by quantitative stereology and three dimensional reconstruction. Protoplasma 81: 77-109.

Banavar, J. R., J. Damuth, A. Maritan, and A. Rinaldo. 2002. Supply-demand balance and metabolic scaling. Proc. Natl. Acad. Sci. USA 99: 10506-10509.

Bauchop, T., and S. R. Elsden. 1960. The growth of micro-organisms in relation to their energy supply. J. Gen. Microbiol. 23: 457-469.

Biswas, S. K., M. Yamaguchi, N. Naoe, T. Takashima, and K. Takeo. 2003. Quantitative three-dimensional structural analysis of *Exophiala dermatitidis* yeast cells by freeze-substitution and serial ultrathin sectioning. J. Electron Microsc. (Tokyo) 52: 133-143.

Brown, J. H., G. B. West, and B. J. Enquist. 2005. Yes, West, Brown and Enquist's model of allometric scaling is both mathematically correct and biologically relevant. Func. Ecol. 19: 735-738.

Burger, J. R., C. Hou, and J. H. Brown. 2019. Toward a metabolic theory of life history. Proc. Natl. Acad. Sci. USA 116: 26653-26661.

Burton, M. D., and J. Moore. 1974. The mitochondrion of the flagellate, *Polytomella agilis.* J. Ultrastruct. Res. 48: 414-419.

Chaui-Berlinck, J. G. 2006. A critical understanding of the fractal model of metabolic scaling. J. Exp. Biol. 209: 3045-3054.

DeLong, J. P., J. G. Okie, M. E. Moses, R. M. Sibly, and J. H. Brown. 2010. Shifts in metabolic scaling, production, and efficiency across major evolutionary transitions of life. Proc. Natl. Acad. Sci. USA 107: 12941-12945.

Dodds, P. S., D. H. Rothman, and J. S. Weitz. 2001. Re-examination of the "3/4-law" of metabolism. J. Theor. Biol. 209: 9-27.

Fenchel, T. 2014. Respiration in heterotrophic unicellular eukaryotic organisms. Protist 165: 485-492.

Frank, S. A. 2016. The invariances of power law size distributions. F1000Res. 5: 2074.

Glazier, D. S. 2015a. Body-mass scaling of metabolic rate: what are the relative roles of cellular versus systemic effects? Biology (Basel) 4: 187-199.

Glazier, D. S. 2015b. Is metabolic rate a universal 'pacemaker' for biological processes? Biol. Rev. Camb. Philos. Soc. 90: 377-407.

Grimes, G. W., H. R. Mahler, and R. S. Perlman. 1974. Nuclear gene dosage effects on mitochondrial mass and DNA. J. Cell Biol. 61: 565-574.

Hatton, I. A., A. P. Dobson, D. Storch, E. D. Galbraith, and M. Loreau. 2019. Linking scaling laws across eukaryotes. Proc. Natl. Acad. Sci. USA 116: 21616-21622.

Hoehler, T. M., and B. B. Jørgensen. 2013. Microbial life under extreme energy limitation. Nat. Rev. Microbiol. 11: 83-94.

Huxley, J. S. 1932. Problems of Relative Growth. Methuen & Co. Ltd., London, UK.

Kempes, C. P., S. Dutkiewicz, and M. J. Follows. 2012. Growth, metabolic partitioning, and the size of microorganisms. Proc. Natl. Acad. Sci. USA 109: 495-500.

Kimura, M., T. Maruyama, and J. F. Crow. 1963. The mutation load in small populations. Genetics 48: 1303-1312.

Kleiber, M. 1932. Body size and metabolism. Hilgardia 6: 315-353.

Kleiber, M. 1947. Body size and metabolic rate. Physiol. Rev. 27: 511-541.

Kozłowski, J., and M. Konarzewski. 2004. Is West, Brown and Enquist's model of allometric scaling mathematically correct and biologically relevant? Func. Ecol. 18: 283-289.

Kozłowski, J., and M. Konarzewski. 2005. West, Brown and Enquist's model of allometric scaling again: the same questions remain. Func. Ecol. 19: 739-743.

Kühlbrandt, W. 2015. Structure and function of mitochondrial membrane protein complexes. BMC Biol. 13: 89.

Lane, N. 2002. Power, Sex, Suicide: Mitochondria and the Meaning of Life. Oxford Univ. Press, Oxford, UK.

Lane, N. 2015. The Vital Question. W. W. Norton & Co., Inc. New York, NY.

Lane N. 2020. How energy flow shapes cell evolution. Curr. Biol. 30: R471-R476.

Lane, N., and W. Martin. 2010. The energetics of genome complexity. Nature 467: 929-934.

Lücken, U., E. P. Gogol, and R. A. Capaldi. 1990. Structure of the ATP synthase complex (ECF1F0) of *Escherichia coli* from cryoelectron microscopy. Biochem. 29: 5339-5343.

Lynch, M. 2020. The evolutionary scaling of cellular traits imposed by the drift barrier. Proc. Natl. Acad. Sci. USA 117: 10435-10444.

Lynch, M., and G. K. Marinov. 2015. The bioenergetic costs of a gene. Proc. Natl. Acad. Sci. USA 112: 15690-15695.

Lynch, M., and G. K. Marinov. 2017. Membranes, energetics, and evolution across the prokaryote-eukaryote divide. ELife 6: e20437.

Lynch, M., and G. K. Marinov. 2018. Reply to Martin and colleagues: mitochondria do not boost the bioenergetic capacity of eukaryotic cells. Biology Direct 13: 26.

Lynch, M., B. Trickovic, W.-C. Ho, and C. P. Kempes. 2020. Evolutionary scaling of maximum growth rates with cell size. Nature Ecol. Evol. (in revision).

Lynch, M., and J. B. Walsh. 1998. Genetics and Analysis of Quantitative Traits. Sinauer Assocs., Inc., Sunderland, MA.

Magalon, A., and F. Alberge. 2015. Distribution and dynamics of OXPHOS complexes in the bacterial cytoplasmic membrane. Biochim. Biophys. Acta 1857: 198-213.

Marañòn, E. 2015. Cell size as a key determinant of phytoplankton metabolism and community structure. Annu. Rev. Mar. Sci. 7: 241-264.

Marañón, E, P. Cermeño, D. C. López-Sandoval, T. Rodriguez-Ramos, C. Sobrino, M. Huete-Ortega, J. M. Blanco, and J. Rodriguez. 2013. Unimodal size scaling of phytoplankton growth and the size dependence of nutrient uptake and use. Ecol. Lett. 16: 371-379.

Marshall, W. F. 2020. Scaling of subcellular structures. Annu. Rev. Cell Dev. Biol. (in press).

Okie, J. G. 2013. General models for the spectra of surface area scaling strategies of cells and organisms: fractality, geometric dissimilitude, and internalization. Am. Nat. 181: 421-439.

Osafune, T., S. Mihara, E. Hase, and I. Ohkuro. 1975. Electron microscope studies of the vegetative cellular life cycle of *Chlamydomonas reinhardi* Dangeard in synchronous culture. III. Three-dimensional structures of mitochondria in the cells at intermediate stages of the growth phase of the cell cycle. J. Electron Microsc. (Tokyo) 24: 247-252.

Pellegrini, M. 1980. Three-dimensional reconstruction of organelles in *Euglena gracilis* Z. I. Qualitative and quantitative changes of chloroplasts and mitochondrial reticulum in synchronous photoautotrophic culture. J. Cell Sci. 43: 137-166.

Pirt, S. J. 1982. Maintenance energy: a general model for energy-limited and energy-sufficient growth. Arch. Microbiol. 133: 300-302.

Pittis, A. A., and T. Gabaldón. 2016 Late acquisition of mitochondria by a host with chimaeric prokaryotic ancestry. Nature 531: 101-104.

Posakony, J. W., J. M. England, and G. Attardi. 1977. Mitochondrial growth and division during the cell cycle in HeLa cells. J. Cell Biol. 74: 468-491.

Rafelski, S. M., M. P. Viana, Y. Zhang, Y. H. Chan, K. S. Thorn, P. Yam, J. C. Fung, H. Li, F. Costa Lda, and W. F. Marshall. 2012. Mitochondrial network size scaling in budding yeast. Science 338: 822-824.

Raven, J. A. 1986. Physiological consequences of extremely small size for autotrophic organisms in the sea, pp. 1-70. *In* T. Platt and E. K. W. Li (eds.) Photosynthetic picoplankton. Can. Bull. Fish. Oceans.

Rosen, D., M. Edelman, E. Galun, and D. Danon. 1974. Biogenesis of mitochondria in *Trichoderma viride:* structural changes in mitochondria and other spore constituents during conidium maturation and germination. Microbiol. 83: 31-49.

Russell, J. B., and G. M. Cook. 1995. Energetics of bacterial growth: balance of anabolic and catabolic reactions. Microbiol. Rev. 59: 48-62.

Savage, V. M., B. J. Enquist, and G. B. West. 2007. Comment on 'A critical understanding of the fractal model of metabolic scaling'. J. Exp. Biol. 210: 3873-3874.

Stock, D., A. G. Leslie, and J. E. Walker. 1999. Molecular architecture of the rotary motor in ATP synthase. Science 286: 1700-1705.

Tempest, D. W., and O. M. Neijssel. 1984. The status of YATP and maintenance energy as biologically interpretable phenomena. Annu. Rev. Microbiol. 38: 459-486.

Thompson, D. A. 1917. On Growth and Form. Cambridge Univ. Press, Cambridge, UK.

Tyn, M. T., and T. W. Gusek. 1990. Prediction of diffusion coefficients of proteins. Biotechnol. Bioeng. 35: 327-338.

Uwizeye, C., J. Decelle, P.-H. Jouneau, B. Gallet, J.-B. Keck, C. Moriscot, F. Chevalier, N. L.

Schieber, R. Templin, G. Curien, Y. Schwab, G. Schoehn, S. C. Zeeman, D. Falconet, and G. Finazzi. 2020. In-cell quantitative structural imaging of phytoplankton using 3D electron microscopy. BioRxiv doi.org/10.1101/2020.05.19.104166.

von Bertalanffy, L. 1957. Quantitative laws in metabolism and growth. Quart. Rev. Biol. 32: 217-231.

West, G. 2017. Scale: the Universal Laws of Growth, Innovation, Sustainability, and the Pace of Life in Organisms, Cities, Economies, and Companies. Penguin Press, London, UK.

West, G. B., J. H. Brown, and B. J. Enquist. 1997. A general model for the origin of allometric scaling laws in biology. Science 276: 122-126.

West, G. B., J. H. Brown, and B. J. Enquist. 1999. The fourth dimension of life: fractal geometry and allometric scaling of organisms. Science 284: 1677-1679.

West, G. B., W. H. Woodruff, and J. H. Brown. 2002. Allometric scaling of metabolic rate from molecules and mitochondria to cells and mammals. Proc. Natl. Acad. Sci. USA 99 Suppl. 1: 2473-2478.

Wieser, W. 1994. Cost of growth in cells and organisms: general rules and comparative aspects. Biol. Rev. 69: 1-33.

Yamaguchi, M., Y. Namiki, H. Okada, Y. Mori, H. Furukawa, J. Wang, M. Ohkusu, and S. Kawamoto. 2011. Structome of *Saccharomyces cerevisiae* determined by freeze-substitution and serial ultrathin-sectioning electron microscopy. J. Electron Microsc. (Tokyo) 60: 321-335.

Zeuthen, E. 1953. Oxygen uptake as related to body size in organisms. Quart. Rev. Biol. 28: 1-12.

Figure 8.1. Distributions of species-specific cell volumes for major phylogenetic groups for which multiple measures are available. Vertical tick marks denote group means, bold and narrow horizontal bars denote standard deviations and ranges. From Lynch et al. (2020).

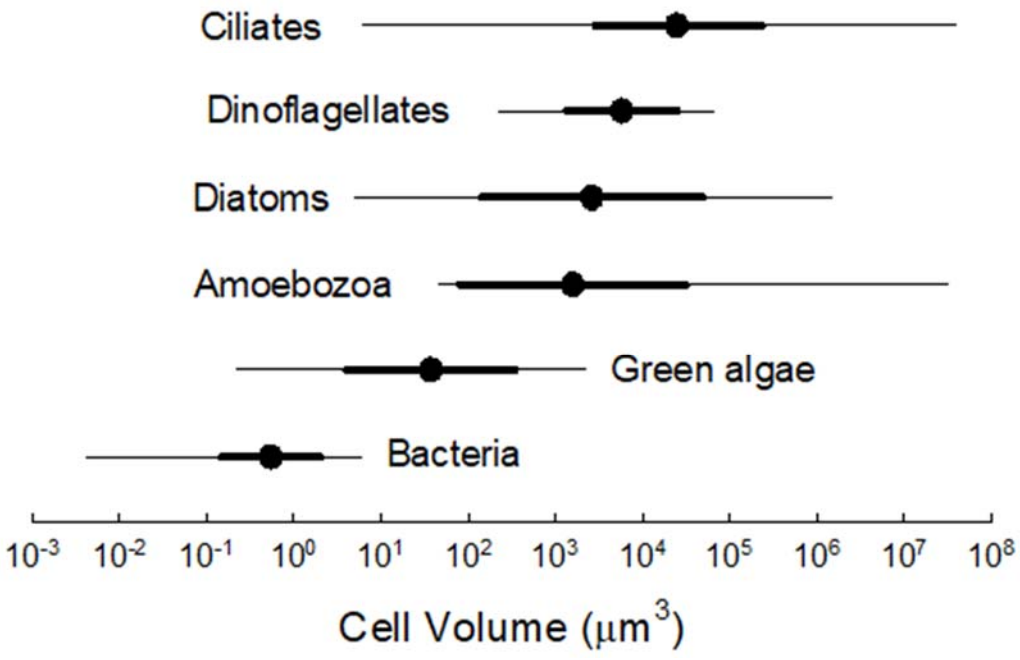

Figure 8.2. Allometric scalings of metabolic rate per cell (M) with cell volume (V) in heterotrophic unicellular species, with units given on the axes: $M = (7.8 \times 10^{-8})V^{1.01}$ (solid black line; standard error of exponent = 0.03); separate regressions for bacteria and unicellular eukaryotes (dashed lines) have slopes of 1.26 and 0.98, respectively, but these are not significantly different. Data are from DeLong et al. (2010) with updated cell volumes derived from the survey in Lynch et al. (2020), and all metabolic rates are scaled to expected values at 20°C.

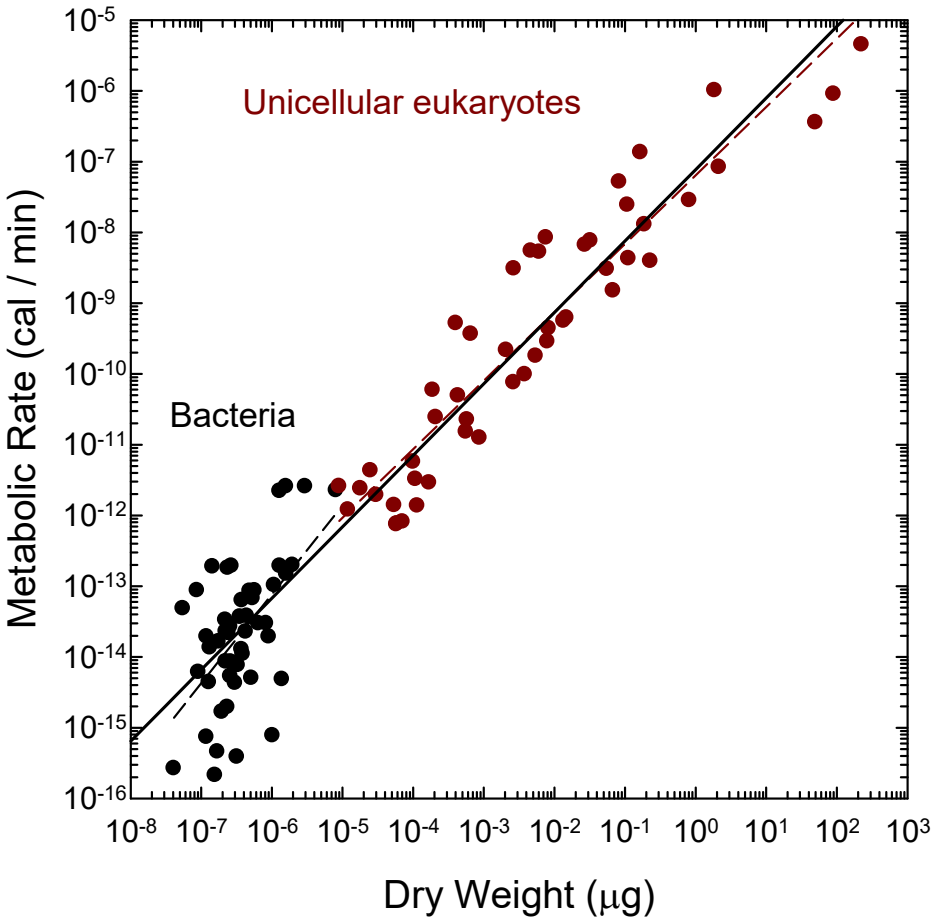

Figure 8.3. **a)** A chemostat (the central vessel) with a continuous input of resources (set by the valve on the upper reservoir containing sterile medium) and outflow (determined by the overflow into the bottom discard container). Aeration ensures an even distribution of cells within the culture and prevents wall growth. **b)** A typical Pirt plot of the rate of glucose consumption by cultures of a bacterium grown at different dilution rates. Note that the measure of resource consumption is in units of glucose / total cell dry weight; this can be converted to ATP consumption per cell using information on the ATP equivalents derived per unit glucose consumed and the dry weight of individual cells. The y-intercept, with units of resource consumed / cell dry weight / time, is a measure of the basal maintenance requirement; the slope, with units of resource consumed / cell division (beyond basal metabolic requirements), is a measure of the total requirements for cell growth.

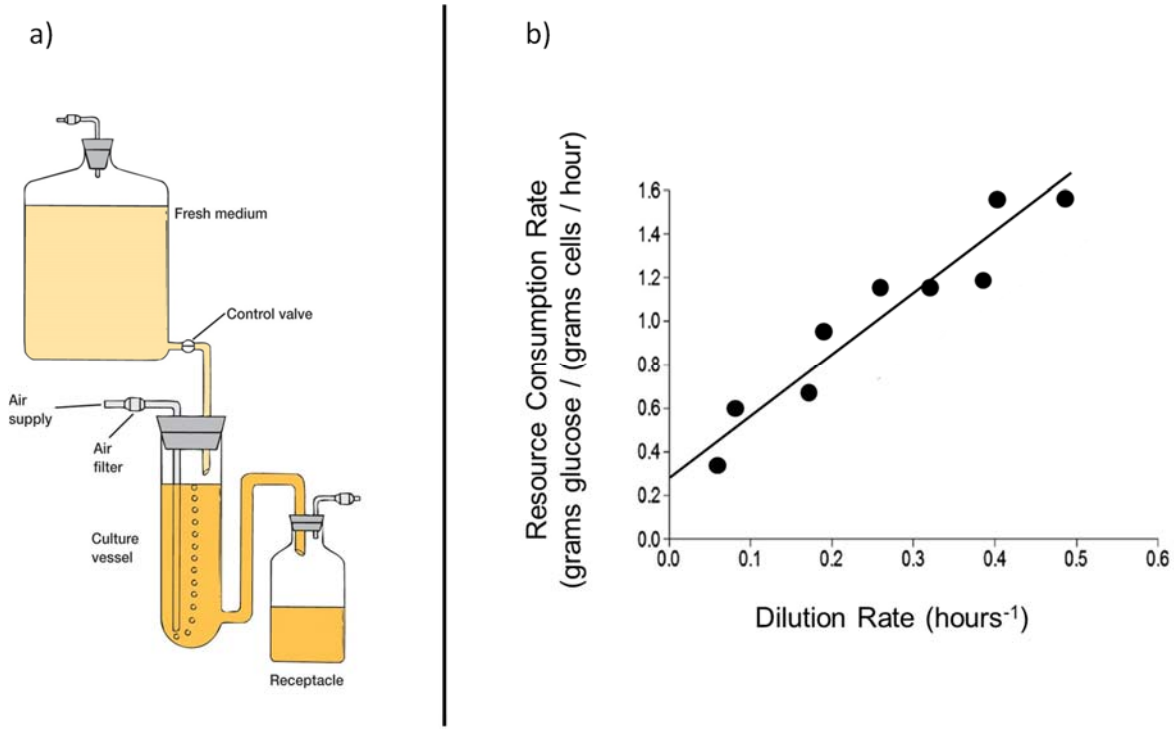

Figure 8.4. Cellular energetic requirements in units of numbers of ATP → ADP hydrolysis events, all scaled to 20°C to normalize results from studies involving different temperatures. Both the maintenance and growth costs for bacterial (black) and unicellular eukaryotic (blue) species are fitted with allometric regression lines. Growth data are available for cell cultures from a few multicellular eukaryotes (red), but these are not included in the regression analysis. From Lynch and Marinov (2015).

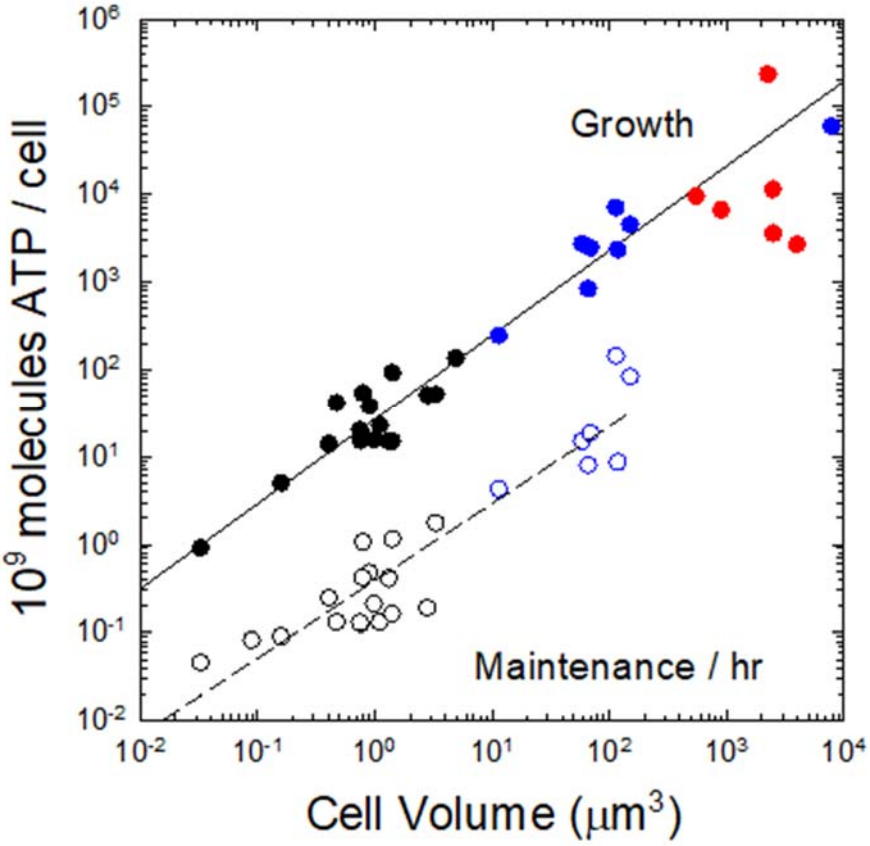

Figure 8.5. Maximum growth rates, $\ln(2)$/doubling time for a) heterotrophic and b) photoautotrophic unicellular species, scaled to expected values at 20°C. Fitted lines are given only for the cases in which the least-squares regression is significant; the slopes are 0.28 for heterotrophic bacteria, -0.21 for amoeboid eukaryotes, -0.22 for ciliates, -0.21 for heterotrophic flagellates (excluding dinoflagellates), -0.19 for dinoflagellates, and -0.09 for both green algae and diatoms. The dashed ellipses envelope the data bacterial and eukaryotic heterotrophs in the upper panel, and are transferred to the lower panel for comparative purposes. From Lynch et al. (2020).

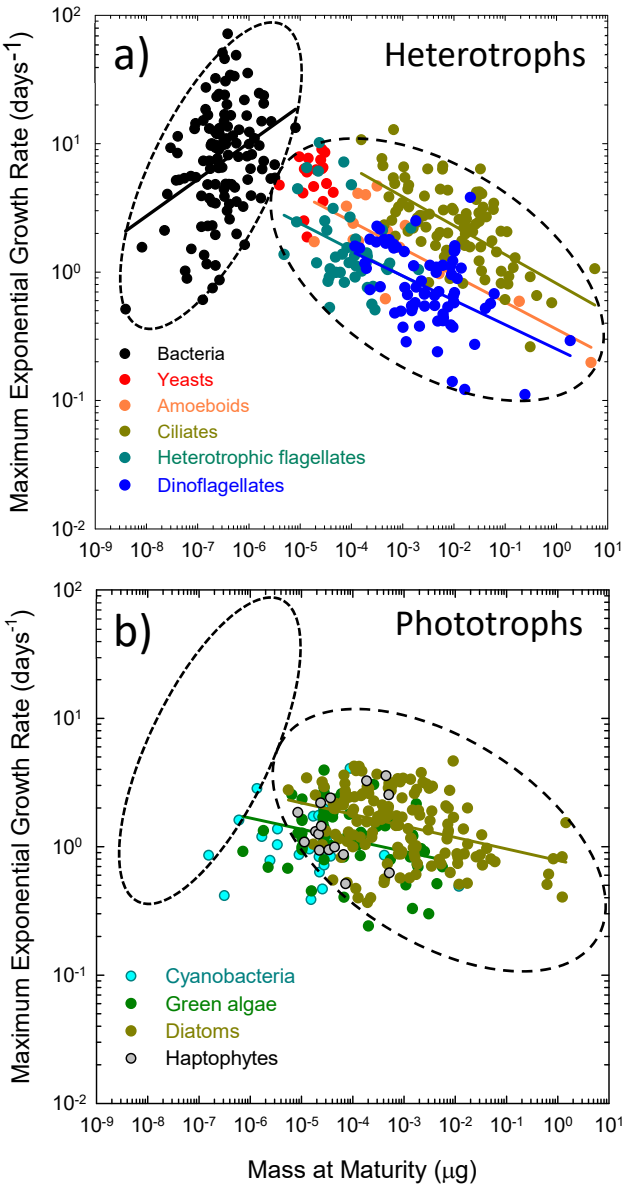

Figure 8.6. Evolutionary long-term average performance (under drift-mutation-selection balance) relative to the maximum value of a trait experiencing an exponential fitness function. Each locus has two possible alleles, + and −, with additive effects on the trait, but with individual fitness declining as e^{-sn}, where s is the selective disadvantage, n is the number of − alleles per individual, and reversible mutation operates between the two alternative alleles at rates u_{01} from − to + and u_{10} from + to −. Populations consist of N haploid individuals. **a)** Results are given for four values of s for the situation in which there is free recombination between sites. Mean performance makes a rapid transition from the neutral expectation $u_{01}/(u_{01}+u_{10})$ at the point at which $1/N = s$. Analytical results are obtained from formulae in Kimura et al. (1963). **b)** Results are given for the situation in which $s = 10^{-6}$, under the assumption of L completely linked genomic sites, all with the same effects. With larger numbers of linked sites, the gradient in mean performance with N becomes more gradual. Here and in panel **d**, the results are obtained by computer simulation using the methods in Lynch (2020). **c)** Modification of the situation in panel **a** to allow for a mixture of unlinked genomic sites with different effects, with various weights given to the four curves in panel **a**. As the population size increases, selection becomes progressively more efficient at promoting alleles with smaller effects. **d)** The situation in which there are blocks of linked loci, one major-effect site with $s = 10^{-5}$, and variable numbers (L) of linked loci with minor effects $s = 10^{-7}$. As L increases, the minor loci contribute proportionally more to total performance, and create background selection interference with the major locus and amongst themselves.

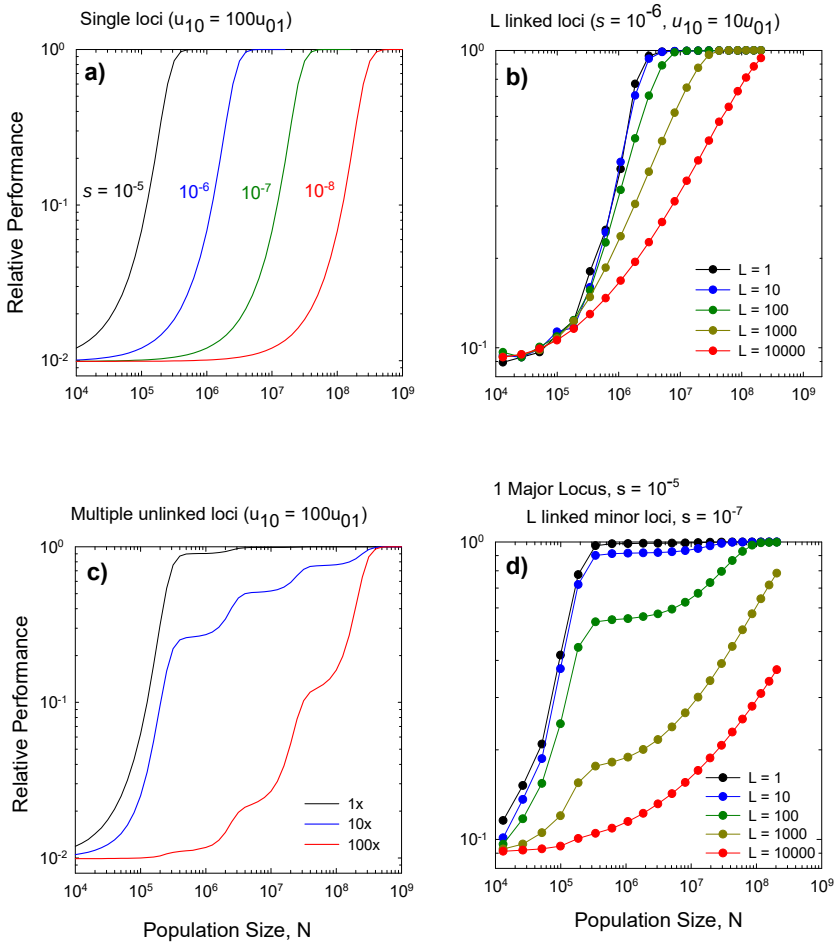

Figure 8.7. a) Relationship between the total outer surface area of mitochondria and that of the plasma membrane for all species with available data. Diagonal lines denote three idealized ratios of the two. Data are from Lynch and Marinov (2017) and Uwizeye et al. (2020). b) The number of ATP synthase complexes per cell scales with cell surface area (S, in μm^2) as $113S^{1.26}$ ($r^2 = 0.99$).

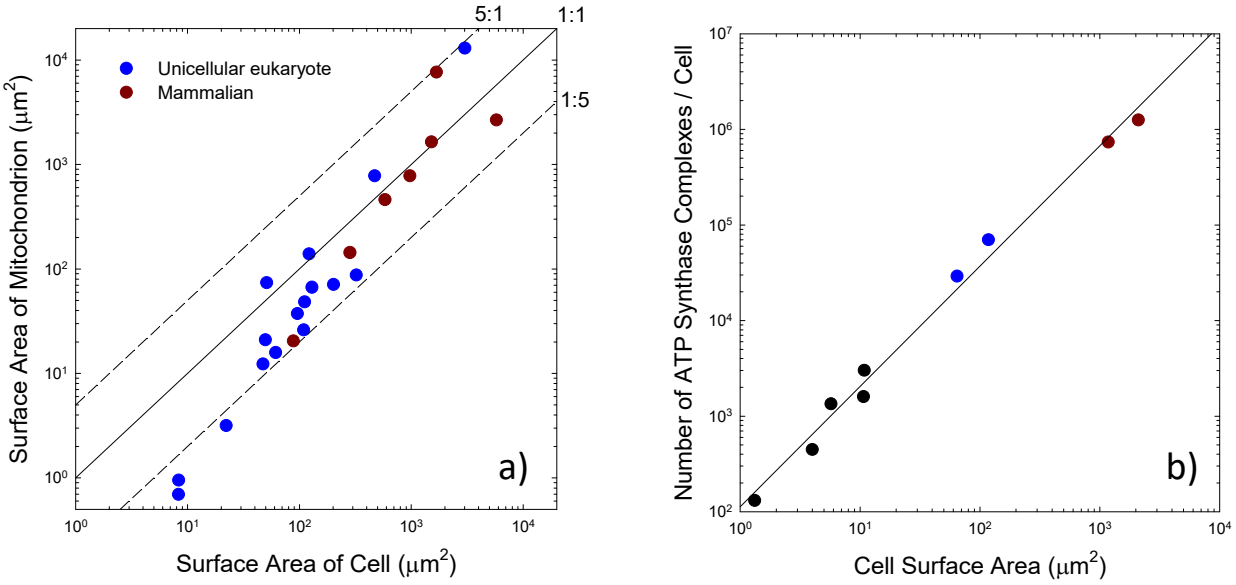

Figure 8.8. The number of ribosomes per cell scales with cell volume (V, in μm^3) as $8551V^{0.79}$ ($r^2 = 0.91$). Color coding as in the previous figure, with green denoting green algae and land-plant cells. From Lynch and Marinov (2017, 2018).